J. Fluid Mech. (2006), *vol.* 562, *pp.* 151–171.
doi:10.1017/S0022112006001054 Printed in the United Kingdom

Vortex equilibrium in flows past bluff bodies

By LUCA ZANNETTI

DIASP, Politecnico di Torino, Corso Duca degli Abruzzi 24, 10129 Torino, Italy

(Received 7 June 2005 and in revised form 25 January 2006)

The equilibrium conditions of a point vortex in the separated flow past a locally deformed wall is studied in the framework of the two-dimensional potential flow. Equilibrium locations are represented as fixed points of the vortex Hamiltonian contour line map. Their pattern is ascribable to the Poincaré–Birkhoff fixed-point theorem. An 'equilibrium manifold', representing the generalization of the Föppl curve for circular cylinders, is defined for arbitrary bodies. The property $\partial\omega/\partial\tilde{\psi}=0$ holds on it, with $\tilde{\psi}$ being the stream function and ω the streamline slope of the pure potential flow.

A 'Kutta manifold' is defined as the locus of vortices in flows that separate at a prescribed point (Kutta condition). The existence of standing vortices that satisfy the Kutta condition is discussed for symmetric bodies. On the basis of an asymptotic expansion of the equilibrium manifold, Kutta manifold and body geometry, it is shown that different classes of symmetric bodies exist which are ranked by the number of allowable standing vortices that satisfy the Kutta condition.

1. Introduction

Inviscid separated flows governed by the Euler equations can have multiple solutions which depend on the multiple allowable distributions of vorticity over the streamlines of the recirculating regions and on the Bernoulli constant jump at their boundaries. For separated regions with closed streamlines, a class of solutions is formed by standing vortex patches which are characterized by constant vorticity and are completely, or partly, embedded in an external potential flow (hereafter simply denoted as 'vortex patches'). Their multiplicity is related to the different allowable values of the area, Bernoulli constant at the boundary and circulation. The Batchelor (1956) flow, which has the property of being the limit of the viscous solution for the Reynolds number going to infinity, is one of these solutions.

The literature on this subject is very extensive. A thorough review and an exhaustive bibliography was provided by Smith (1986). Examples and further references about these solutions have been offered, for example, by Childress (1966), Sadovskii (1971), Deem & Zabusky (1978), Pierrehumbert (1980), Saffman & Tanveer (1982), Chernyshenko (1991), Turfus (1993), Elcrat *et al.* (2000), Crowdy & Marshall (2004).

The main inspiration of the present study is the flow past a semicircular bump, as studied by Elcrat *et al.* (2000), where a rich structure of possible solutions of such a flow is obtained as an evolution of standing point vortices. Point vortices can in fact be considered as vanishing-area vortex regions and vortex patches can be obtained as their accretions. The process of accretion provides a continuum of constant-circulation and increasing-area standing vortex patches. Thus, standing point vortices can be considered as seeds from which vortex patch families grow.

In the flow past a semicircular bump, there is an infinite number of possible standing point vortices. If we restrict the analysis to the solution pertinent to single vortices, the Föppl curve (Föppl 1913) is the locus of such vortices.

Elcrat *et al.* (2000) showed that, for each standing vortex of the Föppl curve, there is a family of vortex patches that starts from the zero-area point vortex to a maximum-area vortex region that is bounded by the solid body. The family elements are vortex patches with the same circulation as the Föppl point vortex and that are embedded in a potential flow with closed streamlines. Thus, the family of recirculating solutions is formed by two-level piecewise-constant-vorticity regions attached to the body. The vorticity is $\omega = 0$ in the outer part and $\omega = \kappa/A_\omega$ in the inner part, with κ being the circulation of the original point vortex and A_ω the area of the inner patch. The point vortex is the extremum element defined by $A_\omega = 0$. The other extremum is the vortex patch that fills the entire region with closed streamlines.

A similar result was obtained by Pierrehumbert (1980) for vortex patches growing from a point-vortex pair. In a similar context, Crowdy & Marshall (2004) have shown that the corotating point-vortex pair and the Rankine vortex are connected by a family of increasing area vortex patches that are in pure solid body rotation.

Thus, point-vortex solutions, besides their significance *per se*, are interesting as starting vortex patch solutions. Moreover, there is the numerical suggestion that if there is no point-vortex solution, there is no vortex-patch solution either. For instance, as discussed in § 5, there is a class of bodies that does not admit standing point vortices which satisfy the Kutta condition (by 'Kutta condition' is meant the requirement that the flow velocity should not be singular at sharp edges). Preliminary numerical results (Gallizio 2004) and ongoing research suggest that standing vortex patches, which satisfy the Kutta condition, are not admitted either.

Point vortices offer a very simple low-order flow model that has been widely used for many purposes. Many results in fluid dynamics have been obtained using this flow model. The literature and textbooks contain many examples and the von Kármán vortex street is one of the most well known of these. More recently, control strategies for vortex shedding suppression have been based on the representation of vortical structures by means of point vortices (Cortelezzi, Chen & Chang 1997; Zannetti & Iollo 2003; Protas 2004). The same simple model was used by Chernyshenko *et al.* (2003) to show the existence, in principle, of bodies free from adverse pressure gradient regions and by Zannetti & Chernyshenko (2005) to design bodies capable of capturing vortices. Meleshko & van Heijst (1994) offered examples in which the highly idealized point-vortex model reveals surprisingly good agreement with experiments.

In this context, the present study addresses the problem of point-vortex equilibrium conditions in the presence of arbitrarily shaped solid boundaries. With an approach similar to Elcrat, Hu & Miller (1997), the classical formulation based on potential flow and conformal mapping is adopted here to study the inviscid flow past arbitrarily shaped bluff bodies. The Hamiltonian character of vortex motion is used to show that the equilibrium positions of vortices are linked to the Poincaré–Birkhoff fixed-point theorem. The Routh (1881) theory on vortex motion is used to show that, in general, a manifold exists which is the locus of the single standing vortices and which can be considered as the generalization of the Föppl curve.

The implications of the Kutta condition, which should be enforced on bodies with sharp edges, lead to the definition of a Kutta manifold, which is the locus of the vortices that satisfy the Kutta condition. The intersections of the Kutta manifold and the equilibrium manifold are the locations of standing vortices that satisfy the Kutta condition. It is known that these intersections may not exist. Smith & Clark (1986),

for instance, showed that a flat plate orthogonal to the flow does not admit standing vortices which satisfy the Kutta condition. This issue is addressed here for arbitrarily shaped bodies.

The paper is organized as follows. In order to elucidate the relationship between the Poincaré–Birkhoff fixed-point theorem and the vortex equilibria, the equilibrium conditions of a point vortex standing in a flow swirling past a cylinder with an arbitrary cross-section are considered in § 2. The study is extended to the flow past infinite bodies in § 3, and to the flow inside a channel in § 4. The Kutta condition issue is analysed in § 5, while § 6 is devoted to the concluding remarks.

2. Swirling flow

Let us first consider an irrotational flow swirling around the unit circle of the complex ζ-plane, with $\zeta = \rho \exp(\mathrm{i}\varphi)$. Let the potential swirling flow be induced by a vortex with circulation Γ located at the unit circle centre $\zeta = 0$. We look for the equilibrium conditions of a point vortex with circulation κ located outside the unit circle in $\zeta = \zeta_0$. The complex potential w_ζ then is

$$w_\zeta = \frac{\Gamma}{2\pi\mathrm{i}} \log(\zeta) + \frac{\kappa}{2\pi\mathrm{i}} \log\left(\frac{\zeta - \zeta_0}{\zeta - 1/\zeta_0^\star}\right)$$

with * denoting the complex conjugate. The complex velocity $\mathrm{d}w_\zeta/\mathrm{d}\zeta$ of fluid particles is

$$\frac{\mathrm{d}w_\zeta}{\mathrm{d}\zeta} = \frac{\Gamma}{2\pi\mathrm{i}} \frac{1}{\zeta} + \frac{\kappa}{2\pi\mathrm{i}} \left(\frac{1}{\zeta - \zeta_0} - \frac{1}{\zeta - 1/\zeta_0^\star}\right)$$

and the conjugate velocity of the free vortex is

$$\dot{\zeta}_0^\star = \frac{\Gamma}{2\pi\mathrm{i}} \frac{1}{\zeta_0} - \frac{\kappa}{2\pi\mathrm{i}} \frac{1}{\zeta_0 - 1/\zeta_0^\star}. \tag{2.1}$$

Equation (2.1) can be rearranged in the form of a one-degree-of-freedom autonomous Hamiltonian dynamical system:

$$\dot{\rho}_0 = \frac{\partial H_\zeta}{\rho_0 \partial \varphi_0}, \qquad \rho_0 \dot{\varphi}_0 = -\frac{\partial H_\zeta}{\partial \rho_0}, \tag{2.2}$$

with H_ζ being the Hamiltonian function:

$$H_\zeta = -\frac{\Gamma}{4\pi} \log(\rho^2) + \frac{\kappa}{4\pi} \log(\rho^2 - 1). \tag{2.3}$$

Since H_ζ is conserved along the vortex trajectories, these, from (2.2) and (2.3), are $\rho = \text{const}$ circles along which the vortex velocity is constant:

$$\dot{\rho}_0 = 0, \quad \dot{\varphi}_0 = \frac{\Gamma}{2\pi} \frac{1}{\rho_0^2} - \frac{\kappa}{2\pi} \frac{1}{\rho_0^2 - 1}. \tag{2.4}$$

For $\Gamma/\kappa \leqslant 1$ and $\kappa < (>) 0$, the free vortex moves counterclockwise (clockwise) along circular trajectories at any flow region point. For $\Gamma/\kappa > 1$ the free vortex stands in equilibrium on the circle with radius

$$\rho_{eq} = \sqrt{\frac{\Gamma/\kappa}{\Gamma/\kappa - 1}}. \tag{2.5}$$

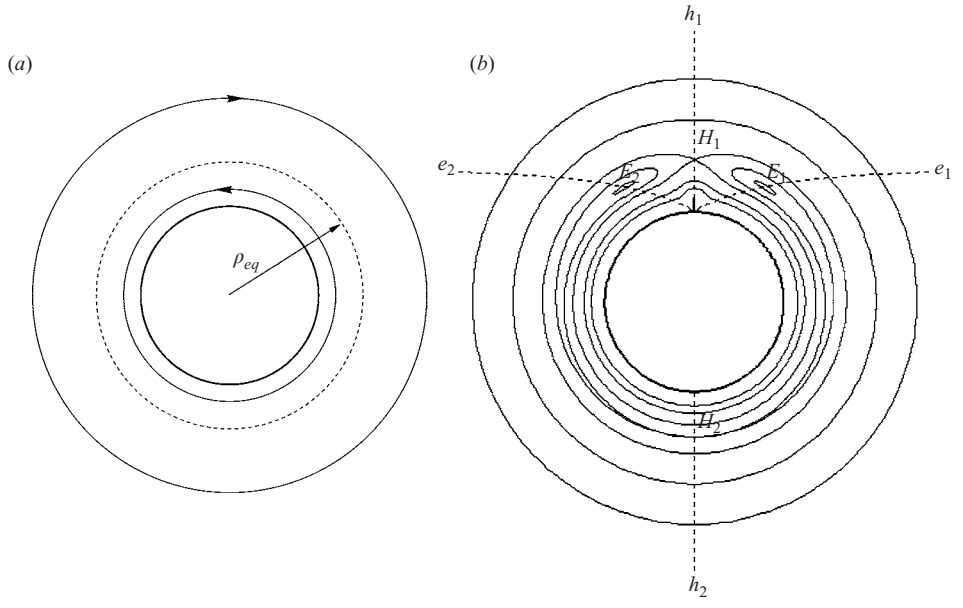

FIGURE 1. Vortex Hamiltonian for $\Gamma/\kappa = 1.8$: (*a*) circular cylinder; (*b*) circular finned cylinder with $\epsilon = 0.01$.

For $\rho < \rho_{eq}$ the vortex moves counterclockwise (clockwise), and clockwise (counterclockwise) for $\rho > \rho_{eq}$. Circular trajectories and the equilibrium circle are shown for $\Gamma/\kappa = 1.8$ on figure 1*a*) .

From the dynamical system theory point of view, the scenario is typical of the twist map, with the $\rho = \rho_{eq}$ circle being a fixed-point locus. According to the Poincaré–Birkoff theorem (see Tabor 1989), the locus of fixed points breaks down under a perturbation and a finite even number of fixed points survives. The surviving fixed-point pattern is alternately made up of elliptic (stable) and hyperbolic (unstable) fixed points.

This is represented on the right hand side of figure 1, with reference to a cylinder with a fin on the top which acts as a flat plate orthogonal to the flow. As discussed hereafter, the equilibrium points for the assigned Γ/κ ratio reduces to the four fixed points of the new Hamiltonian contour map, with H_1 and H_2 being hyperbolic (unstable) fixed points and E_1 and E_2 being elliptic (stable) fixed points.

Let the new perturbed flow be defined on the complex z-plane, with $z = r\exp(\mathrm{i}\vartheta)$. The finned cylinder can be obtained as a conformal representation of the unit circle of the ζ-plane. The proper $z = f(\zeta)$ mapping can be obtained by means of a transformation chain. First, the modified Joukowski mapping

$$\mu(\zeta) = \left(1 + \frac{\epsilon}{2}\right)\left(\zeta - \frac{1}{\zeta}\right) + \mathrm{i}\epsilon$$

maps the unit circle of the ζ-plane onto the flat plate of the μ-plane with extrema at $\mu = -2\mathrm{i}$ and $\mu = 2\mathrm{i}(1+\epsilon)$; then the inverse Joukowski transformation

$$z(\mu) = \frac{\mu + \sqrt{\mu^2 + 4}}{2}$$

maps the flat plate onto the finned unit circle of the z-plane, with the fin extending from $z=\mathrm{i}$ to $z=\mathrm{i}(1+\epsilon+\sqrt{\epsilon^2+2\epsilon})$. The mapping function then becomes

$$f(\zeta)=z(\mu(\zeta)).$$

Since the complex potential is invariant under conformal mapping, the complex potential of the swirling and vortex flow past the finned cylinder is $w_z=w_\zeta(\zeta(z))$, with $\zeta(z)=f^{-1}(z)$.

Let $z_0=f(\zeta_0)$ be the vortex position on the z-plane; according to the Routh (1881) rule (see also Clements 1973; Saffman 1992), the vortex velocity $\dot{z}_0$ is given by

$$\dot{z}_0^\star=\left(\zeta_0'^\star-\frac{\kappa}{4\pi\mathrm{i}}\frac{\mathrm{d}}{\mathrm{d}\zeta_0}\log\frac{\mathrm{d}z_0}{\mathrm{d}\zeta_0}\right)\frac{\mathrm{d}\zeta_0}{\mathrm{d}z_0}, \tag{2.6}$$

with $\zeta_0'^\star$ given by (2.1). If the vortex location on the physical z-plane is expressed by the (ρ_0,φ_0) coordinates of its ζ-plane image, the vortex equilibrium condition $\dot{z}_0^\star=0$ is given by the formula

$$\rho_0\rho_0'-\mathrm{i}\rho_0^2\varphi_0'-\frac{\kappa}{4\pi\mathrm{i}}\zeta_0\frac{\mathrm{d}}{\mathrm{d}\zeta_0}\log\frac{\mathrm{d}z_0}{\mathrm{d}\zeta_0}=0. \tag{2.7}$$

Its real and imaginary parts, together with (2.4), provide the two relationships

$$\mathrm{Im}\left(\zeta_0\frac{\mathrm{d}}{\mathrm{d}\zeta_0}\log\frac{\mathrm{d}z_0}{\mathrm{d}\zeta_0}\right)=0, \tag{2.8}$$

$$\mathrm{Re}\left(\zeta_0\frac{\mathrm{d}}{\mathrm{d}\zeta_0}\log\frac{\mathrm{d}z_0}{\mathrm{d}\zeta_0}\right)=\frac{\Gamma}{\kappa}-\frac{\rho_0^2}{\rho_0^2-1}. \tag{2.9}$$

Equation (2.8) is remarkable as it only depends on the body geometry and is independent of the flow properties. It defines the $z(\rho_0,\varphi_0)_{eq}$ manifold of the vortex equilibrium loci, equivalent to the Föppl curves. Since the Riemann mapping theorem states that any simply connected region can be mapped onto the unit circle of the ζ-plane, (2.8) holds for any cylinder with a simply connected cross-section.

For the flow past the finned circle under consideration, this manifold, mapped on the physical z-plane, is represented by the four branch curves (h_1,e_1,h_2,e_2) shown on figure 1(*b*). For each point $(\rho_0,\varphi_0)_{eq}$ of the manifold, (2.9) provides the Γ/κ ratio pertinent to a standing vortex.

Equation (2.8) provides noticeable geometrical and physical properties of the vortex equilibrium loci. Let us write the mapping derivative $\mathrm{d}z/\mathrm{d}\zeta$ as $\mathrm{d}z/\mathrm{d}\zeta=|\mathrm{d}z/\mathrm{d}\zeta|\exp(\mathrm{i}\omega)$, with ω expressing the local rotation induced by the mapping on the z-plane with respect to the ζ-plane. Equation (2.8) reduces to

$$\frac{\partial\omega}{\partial\rho}=0. \tag{2.10}$$

Moreover, for vanishing free vortex circulation, $\kappa=0$, the complex potential of the pure swirling flow is

$$w_\Gamma=\phi_\Gamma+\mathrm{i}\psi_\Gamma=\frac{\Gamma}{2\pi\mathrm{i}}\log(\zeta).$$

The angle ω can be interpreted as the difference in the slope of the streamlines $\psi_\Gamma=\mathrm{const}$ between the physical z-plane and the transformed ζ-plane, where the streamlines are circles. Hence, from

$$\frac{\mathrm{d}}{\mathrm{d}\zeta}=\frac{\mathrm{d}w_\Gamma}{\mathrm{d}\zeta}\frac{\mathrm{d}}{\mathrm{d}w_\Gamma}=\frac{1}{\zeta}\frac{\Gamma}{2\pi\mathrm{i}}\frac{\mathrm{d}}{\mathrm{d}w_\Gamma}$$

(2.8) can be rewritten as

$$-\mathrm{Im}\left[\frac{\Gamma}{2\pi \mathrm{i}}\frac{\mathrm{d}}{\mathrm{d}w_\Gamma}\left(\log\left|\frac{\mathrm{d}z_0}{\mathrm{d}\zeta_0}\right| + i\omega\right)\right] = \frac{\partial\omega}{\partial\psi_\Gamma} = 0,$$

that is, the vortex equilibrium loci are those points where $\nabla\omega$ is parallel to the pure swirling flow velocity.

Looking at the vortex velocity $\dot{z}_0$ from the dynamical system point of view, the vortex motion is also governed by a Hamiltonian system on the z-plane,

$$\dot{r}_0 = \frac{\partial H_z}{r_0 \partial \vartheta_0}, \qquad r_0\dot{\vartheta}_0 = -\frac{\partial H_z}{\partial r_0}, \tag{2.11}$$

with the Hamiltonian H_z being related to the Hamiltonian H_ζ by the Routh (1881) rule:

$$H_z = H_\zeta + \frac{\kappa}{4\pi}\log\left|\frac{\mathrm{d}z}{\mathrm{d}\zeta}\right|. \tag{2.12}$$

Following the same approach as Zannetti & Franzese (1994), the motion of the vortex on the z-plane can be represented on the ζ-plane by assuming its transformed coordinates (ρ_0, φ_0) to be non-canonical coordinates. The vortex velocity then becomes

$$\dot{\rho}_0 = J\frac{\partial H_z}{\rho_0 \partial \varphi_0}, \qquad \rho_0\dot{\varphi}_0 = -J\frac{\partial H_z}{\partial \rho_0}, \tag{2.13}$$

with $J = |\mathrm{d}\zeta/\mathrm{d}z|^2$. The ϵ power series expansions of H_z and J are

$$H_z = H_\zeta + \epsilon\frac{\kappa}{4\pi}g(\rho_0, \varphi_0) + O(\epsilon^2), \qquad J = 1 - 2\epsilon g(\rho_0, \varphi_0) + O(\epsilon^2)$$

respectively, with

$$g(\rho_0, \varphi_0) = \frac{\partial}{\partial\epsilon}\left|\frac{\mathrm{d}z}{\mathrm{d}\zeta}\right|_{\epsilon=0}.$$

Equations (2.11) therefore reduce to

$$\dot{\rho}_0 = \frac{\partial H_\zeta}{\rho_0\partial\varphi_0} + \epsilon\left[\frac{\kappa}{4\pi}\frac{\partial g(\rho_0, \varphi_0)}{\rho_0\partial\varphi} - 2g(\rho_0, \varphi_0)\frac{\partial H_\zeta}{\rho_0\partial\varphi_0}\right] + O(\epsilon^2),$$

$$\rho_0\dot{\varphi}_0 = -\frac{\partial H_\zeta}{\partial\rho_0} - \epsilon\left[\frac{\kappa}{4\pi}\frac{\partial g(\rho_0, \varphi_0)}{\partial\rho_0} - 2g(\rho_0, \varphi_0)\frac{\partial H_\zeta}{\partial\rho_0}\right] + O(\epsilon^2),$$

that is, to a perturbation of system (2.2). As predicted by the Poincaré–Birkhoff theorem, only a finite even number of fixed points remains in the perturbed system, and these are alternately stable and unstable.

The equilibrium manifold (2.8) is the locus of the vortex equilibria for different Γ/κ values, which are defined by (2.9), while a Hamiltonian manifold (2.3) is pertinent to a single Γ/κ value. The fixed points of the system (2.13) are those points that belong to the equilibrium manifold and satisfy (2.9). Their number does not necessarily match the number of branches of the equilibrium manifold.

The following example elucidates the point by considering a more general quasi-circular body. The geometry has been obtained by taking inspiration from the Theodorsen & Garrick (1934) mapping

$$z = \zeta\exp\sum_{n=0}^{\infty} c_n\zeta^{-n}$$

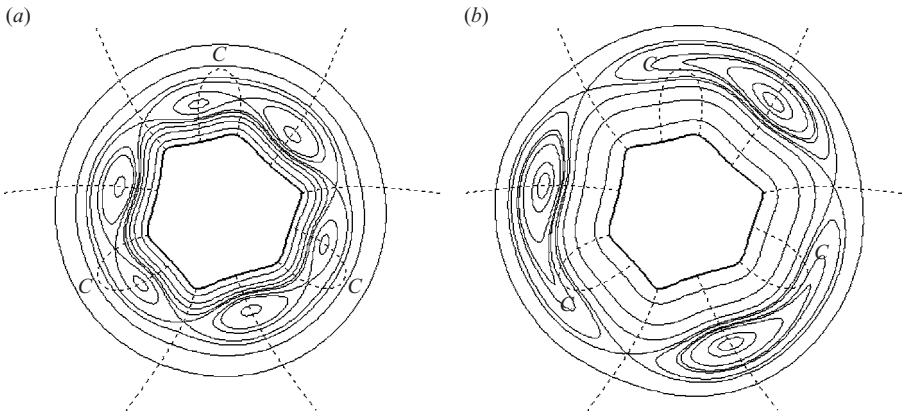

FIGURE 2. Vortex Hamiltonian and equilibrium manifold for a quasi-circular domain: (*a*) $\Gamma/\kappa = 9/5$, (*b*) $\Gamma/\kappa = 4/3$.

which allows a general quasi-circular body of the z-plane to be obtained as conformal mapping of the unit circle of the ζ-plane.

As an example, figure 2 refers to the case where $c_{n\neq 3,6} = 0$, $c_3 = 0.05$, $c_6 = \mathrm{i}0.07$. For this example, two Hamiltonian manifolds have been computed for $\Gamma/\kappa = 9/5$ and $\Gamma/\kappa = 4/3$ and their contour map has been superimposed onto the equilibrium manifold, as shown in figure 2. The equilibrium manifold has six elliptic point branches and six hyperbolic point branches. Three pairs of these branches are connected to each other at points labelled C, and they form three closed lines. The Hamiltonian map pertinent to $\Gamma/\kappa = 9/5$, on figure 2(*a*), shows 12 fixed points, one for each branch of the equilibrium manifold, while for $\Gamma/\kappa = 4/3$, on figure 2(*b*), there are six fixed points. It can be inferred that, for each point C, there is a critical value $4/3 < \Gamma/\kappa < 9/5$ for which a pair of elliptic and hyperbolic points merge at point C and cancel each other.

3. Flow past infinite surfaces

Let us consider a flow past a two-dimensional body which extends to infinity. This is analogous to the previously mentioned swirling flow seen in a scale that is small compared to the cylinder mean radius.

Let us first consider a flow past an infinite flat plate. By assuming the flat plate is coincident with the real axis of the complex ζ-plane, with $\zeta = \xi + \mathrm{i}\eta$, the complex potential w_ζ pertinent to an asymptotic uniform flow with velocity q, parallel to the wall, and to a point vortex, located at $\zeta_0 = \xi_0 + \mathrm{i}\eta_0$ with circulation κ, is

$$w_\zeta = q\zeta + \frac{\kappa}{2\pi\mathrm{i}} \log\left(\frac{\zeta - \zeta_0}{\zeta - \zeta_0^\star}\right). \tag{3.1}$$

As the vortex velocity is

$$\dot{\zeta}_0^\star = q + \frac{\kappa}{4\pi\eta_0}, \tag{3.2}$$

any $\eta_0 = \text{const}$ line is the locus of the equilibrium points for vortices with $\kappa/q = -4\pi\eta_0$. Once the geometry is perturbed, this locus reduces to a finite number of alternating stable and unstable equilibrium points.

As a result of the Riemann mapping theorem, any simply connected flow region bounded by an infinite boundary can be transformed by conformal mapping onto the upper half of the ζ-plane, with the boundary mapped onto the real axis and with the infinity mapped to infinity. Denoting such a mapping by $z = F(\zeta)$, the complex potential w_z on the z-plane is $w_z = w_\zeta(F^{-1}(z))$.

Let us consider the case where $\lim_{z\to\infty} \mathrm{d}z/\mathrm{d}\zeta$ is finite. Without any loss of generality it can be assumed that $\lim_{z\to\infty} \mathrm{d}z/\mathrm{d}\zeta = 1$; therefore q is the asymptotic uniform flow velocity on the z-plane.

According to the previously mentioned Routh rule (2.6), with $\zeta_0'^\star$ given by (3.2), the vortex velocity equilibrium equation is

$$1 + \frac{\kappa}{4\pi q}\left[\frac{1}{\eta_0} + \mathrm{i}\frac{\mathrm{d}}{\mathrm{d}\zeta}\left(\log\frac{\mathrm{d}z}{\mathrm{d}\zeta}\right)\right] = 0. \tag{3.3}$$

Separating the imaginary and real parts, the two following equations are obtained:

$$\mathrm{Re}\left[\frac{\mathrm{d}}{\mathrm{d}\zeta}\left(\log\frac{\mathrm{d}z}{\mathrm{d}\zeta}\right)\right] = 0, \tag{3.4}$$

$$\frac{\kappa}{q} = -\frac{4\pi}{1/\eta_0 - \mathrm{Im}[(\mathrm{d}/\mathrm{d}\zeta)(\log \mathrm{d}z/\mathrm{d}\zeta)]}. \tag{3.5}$$

Equation (3.4) is universal; it only depends on the body shape and defines the vortex equilibrium loci, that is, the generalized Föppl curves, while equation (3.5) defines the κ/q value necessary for a vortex to stand at an equilibrium point.

Such a formulation of vortex velocity and equilibrium conditions is based on the definition of the vortex position by means of its (ξ_0, η_0) coordinates on the transformed ζ-plane. Due to the Riemann mapping theorem, this procedure is general, but not always the most convenient. As shown in what follows, however, it can be rearranged to avoid explicit mention of the ζ-plane.

Let us consider the complex potential $\tilde{w}(z)$ relevant to the pure potential ($\kappa = 0$) flow past the infinite body under consideration. In general, such a $\tilde{w}(z)$ potential can be obtained by conformal mapping or other means (for example, as a distribution of singularities), without any need for the $z = F(\zeta)$ mapping. Since the stream function $\tilde{\psi} = \mathrm{Im}(\tilde{w})$ at the body contour takes the value $\tilde{\psi}_b = 0$, the $\tilde{w}(z)$ complex variable function can be interpreted as the inverse $\zeta = F^{-1}(z)$ mapping:

$$\zeta = \frac{\tilde{w}(z)}{q}. \tag{3.6}$$

In fact it maps the flow region of the z-plane onto the upper half of the ζ-plane, with identical points at infinity, without introducing spurious singularities and with $\lim_{z\to\infty} \mathrm{d}\zeta/\mathrm{d}z = 1$.

The vortex velocity (2.6) can be rearranged as

$$\dot{z}_0^\star = \left\{\left[1 + \frac{\kappa}{4\pi\tilde{\psi}} + \frac{\kappa}{4\pi\mathrm{i}}\frac{\mathrm{d}^2\tilde{w}/\mathrm{d}z^2}{(\mathrm{d}\tilde{w}/\mathrm{d}z)^2}\right]\frac{\mathrm{d}\tilde{w}}{\mathrm{d}z}\right\}_{z=z_0}, \tag{3.7}$$

that is, as a function of (x_0, y_0) vortex coordinates on the physical z-plane.

For $\mathrm{d}\tilde{w}/\mathrm{d}z \neq 0$, the vortex equilibrium equation is

$$1 + \frac{\kappa}{4\pi\tilde{\psi}} + \frac{\kappa}{4\pi\mathrm{i}}\left(\frac{\mathrm{d}^2\tilde{w}/\mathrm{d}z^2}{(\mathrm{d}\tilde{w}/\mathrm{d}z)^2}\right)_{z=z_0} = 0, \tag{3.8}$$

whose imaginary part,

$$\mathrm{Re}\left[\frac{\mathrm{d}^2\tilde{w}/\mathrm{d}z^2}{(\mathrm{d}\tilde{w}/\mathrm{d}z)^2}\right]=0, \tag{3.9}$$

defines the vortex equilibrium manifold, that is, the generalized Föppl curve (3.4). This equation relates the vortex equilibrium to the pure potential flow in a compact and simple way. It suggests the same kinematic property of the vortex equilibrium manifold given by (2.10) for the swirling flow,

$$\frac{\partial\omega}{\partial\tilde{\psi}}=0, \tag{3.10}$$

with ω being the complex velocity argument, $\omega=-\arg(\mathrm{d}\tilde{w}/\mathrm{d}z)$. Equilibrium equation (3.9) can be rearranged as

$$\mathrm{Re}\left[\frac{\mathrm{d}^2\tilde{w}/\mathrm{d}z^2}{(\mathrm{d}\tilde{w}/\mathrm{d}z)^2}\right]=\mathrm{Re}\left[\frac{\mathrm{d}}{\mathrm{d}\tilde{w}}\log\left(\left|\frac{\mathrm{d}\tilde{w}}{\mathrm{d}z}\right|\mathrm{e}^{-\mathrm{i}\omega}\right)\right]=-\frac{\partial\omega}{\partial\tilde{\psi}}=0, \tag{3.11}$$

that is, the equilibrium manifold has the property of being the locus where $\nabla\omega$ is parallel to the streamlines of the pure potential flow.

The real part of (3.8) yields (3.5), written in terms of pure potential flow:

$$\kappa=-\frac{4\pi}{1/\tilde{\psi}+\mathrm{Im}[(\mathrm{d}^2\tilde{w}/\mathrm{d}z^2)/(\mathrm{d}\tilde{w}/\mathrm{d}z)^2]}, \tag{3.12}$$

which allots the values of κ to the equilibrium manifold.

The Hamiltonian nature of vortex motion allows the vortex trajectories to be traced as contour lines of the proper Hamilton function, defined by (2.12), where H_ζ is the Hamiltonian pertinent to the ζ-plane flow, that is, $H_\zeta=q\eta_0+(\kappa/4\pi)\log\eta_0$. The Hamiltonian H_z is therefore expressed by the relationship

$$H_z=q\eta_0+\frac{\kappa}{4\pi}\log\eta_0+\frac{\kappa}{4\pi}\log\left|\frac{\mathrm{d}z}{\mathrm{d}\zeta}\right| \tag{3.13}$$

which depends on the (ξ_0,η_0) vortex position on the transformed ζ-plane. Following the same reasoning as above, it can be expressed on the physical z-plane as

$$H_z=\tilde{\psi}+\frac{\kappa}{4\pi}\log\tilde{\psi}-\frac{\kappa}{4\pi}\log\left|\frac{\mathrm{d}\tilde{w}}{\mathrm{d}z}\right|. \tag{3.14}$$

3.1. *Equilibrium manifold and vortex trajectory examples*

As an example of equilibrium manifold detection and vortex trajectory tracing, let us consider a flow past a flat surface with an orthogonal flat plate. Let this body be represented by the real axis of the complex z-plane and by the imaginary axis segment $0\leqslant y\leqslant 1$. The mapping

$$z=\sqrt{\zeta^2-1} \tag{3.15}$$

transforms this body onto the real axis of the ζ-plane. Figure 3, shows the equilibrium manifold inferred from (3.4), and the Hamiltonian contour lines for a vortex standing at an equilibrium point.

The vortex has been selected by assuming its ζ-plane abscissa as $\xi_0=3$; from a trial and error procedure on (3.4) its ordinate is $\eta_0=1.633$. From (3.5) its circulation is $\kappa/q=-21.440$, with the plate height assumed as the reference length. Its location mapped back on the z-plane is $z_0=2.871+1.706\,\mathrm{i}$. The Hamiltonian contour line

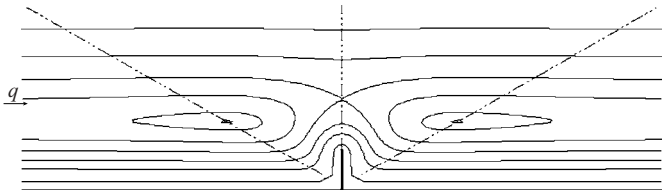

FIGURE 3. Vortex Hamiltonian contour lines (solid) and equilibrium manifold (dash-dot) for an orthogonal flat plate.

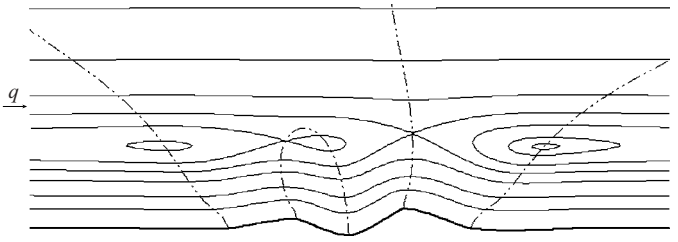

FIGURE 4. Vortex Hamiltonian contour lines (solid) and equilibrium manifold (dash-dot) for an arbitrary wall.

pattern shows that the selected vortex has an elliptic, that is stable, fixed point on the selected point of the right-hand branch of the equilibrium manifold. It has two other equilibrium points: an unstable one at the hyperbolic fixed point belonging to the central branch and a stable one at the elliptic point belonging to the left-hand branch. Below the separatrix, the vortex moves from right to left, above it from left to right and in between the vortex follows closed orbits encircling the elliptic fixed points. The scenario strongly resembles that of the swirling flow past a finned cylinder shown in figure 1. The three stable and unstable alternating fixed points of figure 3 can be seen as the surviving fixed points among the $y = y_{eq} = -\kappa/(4\pi q)$ equilibrium locus relevant to the flow past a flat plate. These are analogous to the upper three fixed points of figure 1. Since the separatrix reconnects at infinity, there is not a fourth fixed point that corresponds to the fourth fixed point of the swirling flow.

A second example is shown in figure 4. The flow past an arbitrarily shaped wall is considered on the z-plane. The real axis of the ζ-plane has been mapped onto the wall according to the following mapping chain that includes a variant of the Theodorsen–Garrick mapping:

$$z = \frac{h(\zeta) + 1}{\mathrm{i}h(\zeta) + 1}$$

with

$$h(\zeta) = \frac{\zeta - \mathrm{i}}{\zeta + \mathrm{i}} \exp \sum_{j=0}^{\infty} a_j \left(\frac{\zeta - \mathrm{i}}{\zeta + \mathrm{i}} \right)^{-j}$$

and with the a_j coefficients determined according to the Ives (1976) method.

The equilibrium manifold presents five branches, with a pair of stable and unstable branches connected to each other. In a way similar to the swirling flow of figure 2, there are five equilibrium points for the κ/q values above a critical value, as shown in figure 4, and three for values below it.

The third example reproduces the Föppl solution pertinent to the flow past a semicircular obstacle. Assuming a unit radius, the complex potential of the pure

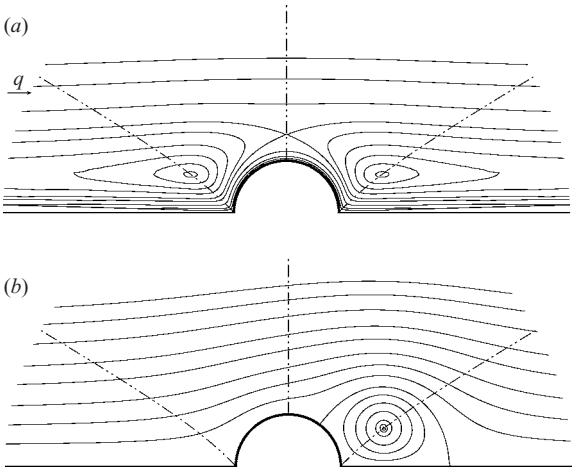

FIGURE 5. Equilibrium manifold, vortex Hamiltonian (*a*) and streamlines (*b*) for a semicircular obstacle.

potential flow is

$$\tilde{w} = qz + \frac{q}{z}.$$

Equation (3.9) yields

$$x[(x^2 + y^2 - 1)^2 - 4y^2(x^2 + y^2)] = 0,$$

that is, the vortex equilibrium manifold is formed by the imaginary axis ($x = 0$) and by the original Föppl curves

$$2y = r - \frac{1}{r},$$

with $r = \sqrt{x^2 + y^2}$. According to (3.14), the Hamiltonian pertinent to a free point vortex is

$$H_z = qy\left(1 - \frac{1}{x^2 + y^2}\right) + \frac{\kappa}{4\pi}\log\left[\left(y - \frac{y}{x^2 + y^2}\right)\left|\frac{(x + \mathrm{i}y)^2}{(x + \mathrm{i}y)^2 - 1}\right|\right].$$

The equilibrium manifold, Hamiltonian contour lines and flow streamlines are represented in figure 5. Assuming the cylinder radius as the reference length, the vortex is located at $r = 2$, that is, $x_0 = 1.854$, $y_0 = 0.75$; the vortex circulation, provided by (3.12), is $\kappa/q = -8.836$.

4. Channel flow

The previous analysis can be extended to a flow past a bluff body that protrudes from a wall of a two-dimensional channel. Let us consider the channel as infinite and represent it on the complex z-plane. By conformal mapping, it can be transformed onto the strip $0 \leqslant \eta \leqslant \pi$ of the complex ζ-plane, whose width is $d = \pi$. For a vortex located at ζ_0, the complex potential on the ζ-plane is

$$w_\zeta = q\zeta + \frac{\kappa}{2\pi\mathrm{i}}\log\left\{\frac{\sinh[(\zeta - \zeta_0)/2]}{\sinh[(\zeta - \zeta_0^\star)/2]}\right\} \tag{4.1}$$

where $q = Q/\pi$, with Q the channel mass flow. The complex velocity on the ζ-plane then becomes

$$\frac{\mathrm{d}w_\zeta}{\mathrm{d}\zeta} = q + \frac{\kappa}{2\pi\mathrm{i}}\left\{\frac{1}{2\tanh[(\zeta-\zeta_0)/2]} - \frac{1}{2\tanh[(\zeta-\zeta_0^\star)/2]}\right\} \tag{4.2}$$

and the vortex velocity on the ζ-plane is

$$\dot{\zeta}_0^\star = \lim_{\zeta\to\zeta_0}\left[\frac{\mathrm{d}w_\zeta}{\mathrm{d}\zeta} - \frac{1}{\zeta-\zeta_0}\right] = q + \frac{\kappa}{4\pi}\frac{1}{\tan\eta_0}. \tag{4.3}$$

The vortex velocity on the physical z-plane is given by the Routh rule (2.6). It follows that, since $\dot{\zeta}_0^\star$ is a real quantity, the vortex equilibrium manifold is expressed in the channel flow by the same equation (3.4),

$$\mathrm{Re}\left[\frac{\mathrm{d}}{\mathrm{d}\zeta}\left(\log\frac{\mathrm{d}z}{\mathrm{d}\zeta}\right)\right] = 0,$$

as for the flow past an infinite surface. The vortex strength at the equilibrium points is obtained by setting the real part of vortex velocity (2.6) to zero:

$$\frac{\kappa}{q} = -\frac{4\pi}{1/\tan\eta_0 - \mathrm{Im}[(\mathrm{d}/\mathrm{d}\zeta)(\log\mathrm{d}z/\mathrm{d}\zeta)]_{\zeta=\zeta_0}}. \tag{4.4}$$

The Hamiltonian H_z on the physical z-plane can be obtained by the Routh rule as expressed by (2.12), with the ζ-plane Hamiltonian H_ζ being

$$H_\zeta = q\eta_0 + \frac{\kappa}{4\pi}\log(\sin\eta_0).$$

The vortex equilibrium manifold and Hamiltonian can be obtained directly on the z-plane by using the same artifice employed in the case of the flow past an infinite surface, that is, by setting

$$\zeta = \frac{\tilde{w}(z)}{q}, \tag{4.5}$$

where $\tilde{w}(z)$ is the complex potential of the pure potential flow. Recasting (2.6) and (4.3), the vortex velocity becomes

$$\dot{z}_0^\star = \left[\left(1 + \frac{\kappa}{4\pi}\frac{1}{\tan\tilde{\psi}} + \frac{\kappa}{4\pi\mathrm{i}}\frac{\mathrm{d}^2\tilde{w}/\mathrm{d}z^2}{(\mathrm{d}\tilde{w}/\mathrm{d}z)^2}\right)\frac{\mathrm{d}\tilde{w}}{\mathrm{d}z}\right]_{z=z_0}. \tag{4.6}$$

The vortex equilibrium manifold is defined by its imaginary part, which yields the same equation (3.9) as for the flow past an infinite wall. Equation (3.11) also holds, with the same kinematic meaning.

The vortex intensity on the equilibrium manifold is given by

$$\kappa = -\frac{4\pi}{1/\tan\tilde{\psi} + \mathrm{Im}[(\mathrm{d}^2\tilde{w}/\mathrm{d}z^2)/(\mathrm{d}\tilde{w}/\mathrm{d}z)^2]}. \tag{4.7}$$

In terms of pure potential flow, the vortex Hamiltonian is

$$H_z = \tilde{\psi} + \frac{\kappa}{4\pi}\log[\sin(\tilde{\psi}/q)] - \frac{\kappa}{4\pi}\log\left|\frac{\mathrm{d}\tilde{w}}{\mathrm{d}z}\right|. \tag{4.8}$$

4.1. *Channel flow example*

The flow past a plate protruding from a wall of a constant-width channel is considered. As shown in figure 6, the flow region can be obtained as a conformal map of a strip

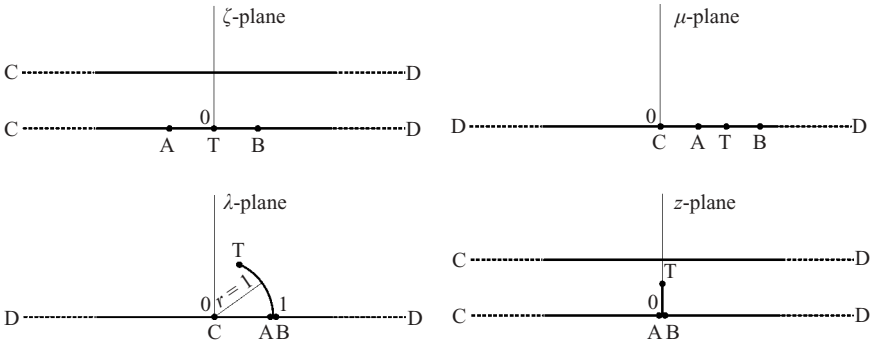

FIGURE 6. $\zeta\text{-} \rightarrow \mu\text{-} \rightarrow \lambda\text{-} \rightarrow z$-plane mapping chain.

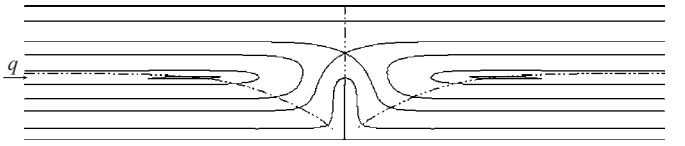

FIGURE 7. Vortex equilibrium manifold and Hamiltonian contour lines for an orthogonal flat plate inside a channel.

of the ζ-plane. The mapping can be summed in a sequence of steps. The strip of the ζ-plane is mapped by $\mu = \exp(\zeta)$ onto the upper half-μ-plane; then the real axis segment A $-$ B of the μ-plane is mapped, by elementary mapping, onto a circular arc of the λ-plane and the z-plane channel is obtained from $z = \log \lambda$.

The location of the circular arc centre λ_c on the λ-plane defines the plate camber on the z-plane; the plate reduces to a flat plate for $\lambda_c = 0$, as shown in the figure, while for $\lambda_c < (>) 0$ the plate is concave on its right(left)-hand side.

Figure 7 shows the vortex equilibrium manifold and the Hamilton function contour lines for the flat plate case and for the vortex circulation $\kappa/q = -133.043$, with d/π assumed as the reference length.

5. Kutta condition

When the body presents a sharp edge, the Kutta condition has to be enforced in order to avoid a velocity singularity, that is, the separation has to occur at the edge. The vortex equilibrium points are therefore reduced from an infinite to a finite or null number. For instance, in the case of the flow past an orthogonal flat plate considered in § 2, it has been proved by Smith & Clark (1986) that there are no equilibrium points for Kutta-condition-satisfying vortices. In Zannetti & Iollo (2003), it was argued that this non-existence is related to the symmetry. It was shown that once the symmetry of the orthogonal flat plate is broken by bending the plate or by applying suction, standing vortices that satisfy the Kutta condition exist. In his original paper, Föppl (1913) observed this non-existence and cited the work of Prandtl, stating existence for bent plates. Incidentally, the Föppl assertion on non-existence, though correct, was proved by a fallacious argument that neglects the Routh rule on vortex equilibria.

The same kind of result can be observed for a plate inside a channel, as described in the previous section. Standing point-vortex solutions that satisfy the Kutta condition can be found for cambered plates inside a channel: the lower the camber, the greater

the vortex circulation and the further away its location. On the other hand a flat plate does not admit a standing vortex which satisfies the Kutta condition.

These channel considerations have some relevance to the vortex-patch solutions that, in § 1, were related to point-vortex solutions. It has been mentioned that the point-vortex solution can be considered as the first element of a family of constant circulation and increasing area vortex patches whose last element is partially bounded by the solid boundary. The non-existence of a point-vortex solution could suggest the non-existence of the entire family, that is, of a finite-area wake. Turfus (1993) describes an attached vortex patch in the flow past a flat plate in a channel that contradicts this conjecture. However, Turfus (1993) himself casts some doubt on the convergence of his numerical process. An attempt to replicate his results was made by Gallizio (2004), who confirmed the difficulties involved in assessing a converging numerical solution for a finite-area wake. This is worthy of further investigation.

This symmetry issue, besides its intriguing theoretical interest, has practical relevance, since a symmetric bluff body capable of capturing a steady vortex when the flow reverses could be useful.

In what follows it is shown that, in addition to the orthogonal plate, there are other symmetric bodies that cannot satisfy the Kutta and vortex equilibrium conditions simultaneously. It is proved that the symmetric Ringleb snow cornice (Ringleb 1961) is among such bodies. Several other examples can be provided which show that standing vortices past symmetric bodies do not exist, with the separation taking place from the body point on the axis of symmetry. In his original paper, Föppl observed that this is the case for a semicircular obstacle. Cai, Liu & Luo (2003) observed the same result for semielliptic bodies.

These results might suggest that symmetry in general does not allow for standing vortices with a symmetric separation point. In what follows it is argued that this is true for a certain class of symmetric bodies, but that other classes of symmetric bodies exist with allowed numbers of standing vortices that satisfy the Kutta condition ranging from one to infinity.

Let us map the body under consideration onto the real axis of the ζ-plane with the cusp z_T mapped onto $\zeta = \zeta_T = 0$. The complex velocity on the ζ-plane is

$$\frac{\mathrm{d}w_\zeta}{\mathrm{d}\zeta} = q + \frac{\kappa}{2\pi \mathrm{i}}\left(\frac{1}{\zeta - \zeta_0} - \frac{1}{\zeta - \zeta_0^\star}\right), \tag{5.1}$$

and the Kutta condition $(\mathrm{d}w_\zeta/\mathrm{d}\zeta)_{\zeta=0} = 0$ is expressed by the equation

$$\frac{\kappa}{q} = -\pi \frac{\xi_0^2 + \eta_0^2}{\eta_0}. \tag{5.2}$$

Using (3.5), one obtains

$$\xi_0^2 - 3\eta_0^2 - \eta_0\left(\xi_0^2 + \eta_0^2\right) \mathrm{Im}[(\mathrm{d}/\mathrm{d}\zeta)(\log \mathrm{d}z/\mathrm{d}\zeta)]_{\zeta_0} = 0; \tag{5.3}$$

thus, a (ξ_0, η_0) manifold is defined that will be denoted the 'Kutta manifold' in what follows. The intersections of the equilibrium manifold (3.4) with the Kutta manifold are the positions of standing vortices that satisfy the Kutta condition.

The Ringleb snow cornice (Ringleb 1961) is obtained by mapping the upper half-ζ-plane onto the z-plane by means of the transformation $z = g(\zeta; \zeta_1)$:

$$z = \zeta + \frac{\zeta_1^2}{\zeta - \zeta_1}. \tag{5.4}$$

Let the complex parameter ζ_1 be $\zeta_1 = a + \mathrm{i}b$. For $b < 0$, the upper half of the ζ-plane is mapped onto a region of the z-plane bounded by a cusped line extending to infinity. The cusp corresponds to $\zeta = \zeta_T = 0$ and is located at $z_T = -\zeta_1$.

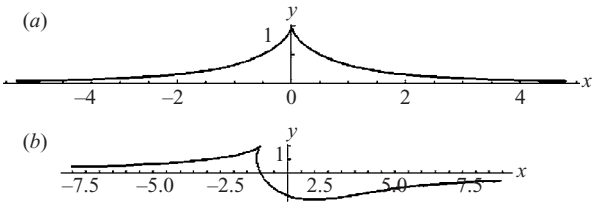

FIGURE 8. Ringleb snow cornices: (*a*) $\epsilon = 0$, (*b*) $\epsilon = 0.5$.

Since $kz = g(k\zeta, k\zeta_1)$, altering ζ_1 by a factor k has the effect of changing the scale and not the shape of the cusped boundary; therefore the shape family defined by the mapping depends on the single parameter a/b. Moreover, for $a = 0$, the cusped line is symmetric. Let us assume $\zeta_1 = \epsilon - \mathrm{i}$. Figure 8 shows the $\epsilon = 0$ and $\epsilon = 0.5$ shapes.

For $\epsilon = 0$, the equilibrium manifold (3.4) on the ζ-half-plane ($\eta_0 > 0$) has three branches expressed by the equations

$$\xi_0 = 0, \tag{5.5a}$$

$$\eta_0 = -1 - \frac{\sqrt{1+\xi_0^2}}{\sqrt{3}} \qquad (\xi_0 < -\sqrt{2}), \tag{5.5b}$$

$$\eta_0 = -1 + \frac{\sqrt{1+\xi_0^2}}{\sqrt{3}} \qquad (\xi_0 > \sqrt{2}). \tag{5.5c}$$

In order to discuss physically reasonable flows, we look for standing vortices that are pertinent to flows that separate at the cusp and reattach downstream, that is, for $q > 0$, for vortices standing on the branch given by (5.5*c*), whose substitution into the Kutta manifold (5.3) yields

$$\left(1+2\xi_0^2\right)\sqrt{3\left(1+\xi_0^2\right)} - 2\left(1+\xi_0^2\right) = 0$$

which does not have real roots for $\xi_0 > \sqrt{2}$. Therefore, there are no standing vortices that satisfy the Kutta condition in the flow past the symmetric Ringleb snow cornice.

Conversely, for $\epsilon \neq 0$, the snow cornice is not symmetric and there are standing vortices that satisfy the Kutta condition. Figure 9 shows the case where $\epsilon = 0.5$, in which the equilibrium and Kutta manifolds intersect. On figure 9(*a*), the Hamiltonian contour lines show that the intersection occurs at a stable equilibrium position; on figure 9(*b*) the streamline pattern shows that the Kutta condition is satisfied.

As previously mentioned, these results might suggest the non-existence of standing vortices with symmetric separation points in a flow past symmetric bodies. This is not the case if we consider that the flow past an infinite flat plate has a locus of such vortices. If the plate is represented as the real axis of the ζ-plane, the line

$$\eta = \frac{\xi}{\sqrt{3}} \tag{5.6}$$

is the locus of standing vortices with circulation

$$\frac{\kappa}{q} = -\pi\frac{\xi_0^2 + \eta_0^2}{\eta_0}, \tag{5.7}$$

which are all pertinent to flows separating on $\zeta = 0$.

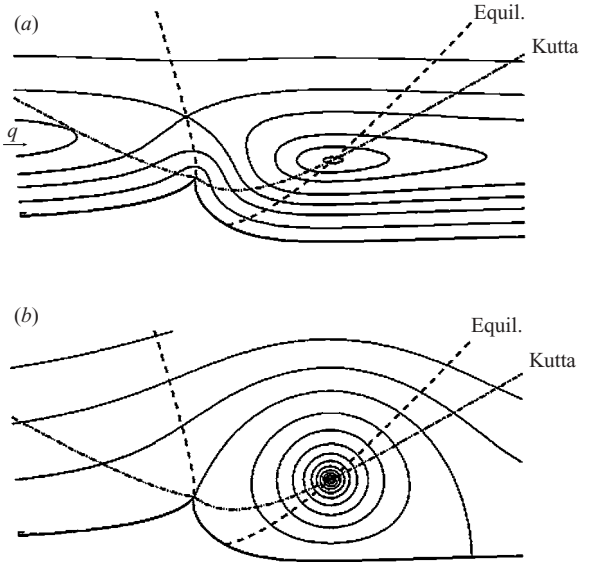

FIGURE 9. (*a*) Hamiltonian, (*b*) streamlines, equilibrium and Kutta manifolds for a non-symmetric Ringleb snow cornice.

In general, the transformation that maps the upper half of the ζ-plane onto a region bounded by a line extending to infinity can be written as

$$z = \zeta + \sum_{n=1}^{\infty} \frac{c_n}{(\zeta - \zeta_1)^n}. \tag{5.8}$$

In order to represent bodies which have the imaginary axis as the symmetry line, let us assume ζ_1 as pure imaginary. Thus, the c_n coefficients should be real/imaginary for odd/even n.

Let N denote the index of the first non-null c_n coefficient in the series (5.8). Here we show that standing vortices have little chance of satisfying the Kutta condition for $N = 1$, but this chance increases for $N > 1$. The argument is based on the asymptotic far-field behaviour of the equilibrium manifold (3.4) and the Kutta manifold (5.3). Since for $\zeta \to \infty$, $z = \zeta$, the far-field asymptotic behaviour on the z-plane is the same as on the ζ-plane. The equilibrium and Kutta manifold series expansions are

$$\mathrm{Re}\left[N(N+1)\frac{c_N}{\zeta^{N+2}} + O\left(\frac{1}{\zeta}\right)^{N+3}\right] = 0, \tag{5.9}$$

$$\xi^2 - 3\eta^2 - \eta(\xi^2 + \eta^2)\mathrm{Im}\left[N(N+1)\frac{c_N}{\zeta^{N+2}} + O\left(\frac{1}{\zeta}\right)^{N+3}\right] = 0 \tag{5.10}$$

respectively. Thus, asymptotic directions (φ_{eq}) of the equilibrium manifold branches are defined by $\mathrm{Re}(c_N \zeta^{-(N+2)}) = 0$, that is,

$$(N+2)\varphi_{eq} = j\frac{\pi}{2} + m\pi$$

with $j = 0$ for even N, $j = 1$ for odd N and $m = 0, 1, 2, \ldots$. If this analysis is restricted to the first quadrant, the Kutta manifold has a unique branch whose asymptote for

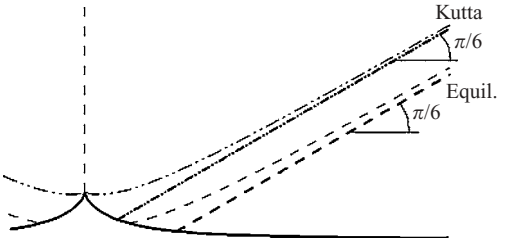

FIGURE 10. Kutta and equilibrium manifolds and asymptotes for a symmetric Ringleb snow cornice.

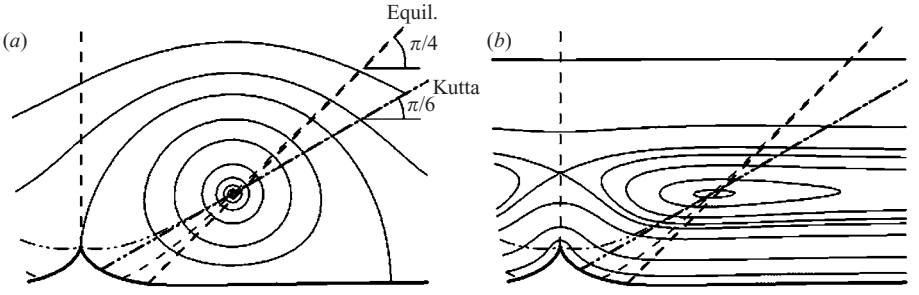

FIGURE 11. Kutta and equilibrium manifolds and asymptotes for $N=2$ cornice. (a) streamlines, (b) Hamiltonian contour lines for $\kappa/q=-16.411$.

any value of N is the line $\eta=\xi/\sqrt{3}$, that is, the line with direction

$$\varphi_{Kutta}=\frac{\pi}{6}.$$

Hence, for $N=1$, the asymptotes of the equilibrium and Kutta manifolds are parallel ($\varphi_{eq}=\varphi_{Kutta}=\pi/6$) with little chance of intersecting. All the previously considered examples of symmetric bodies, that is the symmetric Ringleb snow cornice, orthogonal plate, semicircle and semiellipses, belong to this $N=1$ class. For $N>1$ the asymptotic directions of the equilibrium and Kutta manifolds are different and have greater chances of intersecting.

Examples supporting this statement are provided if we consider the bodies defined by the mapping

$$z=\zeta+\frac{(-\zeta_1)^{N+1}}{N(\zeta-\zeta_1)^N}. \tag{5.11}$$

In its series expansion (5.8) all the coefficients c_n are null except for $n=N$. Assuming $\mathrm{Im}(\zeta_1)<0$, it maps the upper ζ-half-plane onto a region extending to infinity bounded by a cusped line that, for $N=1$, coincides with the Ringleb snow cornice. The cusp is located at $z_T=z(0)$ and the boundary is symmetric for $\mathrm{Re}(\zeta_1)=0$. Let us set $\zeta_1=-\mathrm{i}$; hereafter the reference length on the physical z-plane is $N|z_T|$.

Figure 10 shows the equilibrium and Kutta manifolds and their asymptotes for $N=1$, that is, for the symmetric Ringleb snow cornice. The manifold behaviour confirms the non-existence of standing vortices that satisfy the Kutta condition, as previously proved. The behaviour of the equilibrium and Kutta manifolds for an orthogonal plate, semicircle and semiellipse are very similar to those shown here.

For $N=2$, the equilibrium manifold has a stable equilibrium branch on the first quadrant with an asymptote defined by $\varphi_{eq}=\pi/4$. As shown in figure 11, it intersects

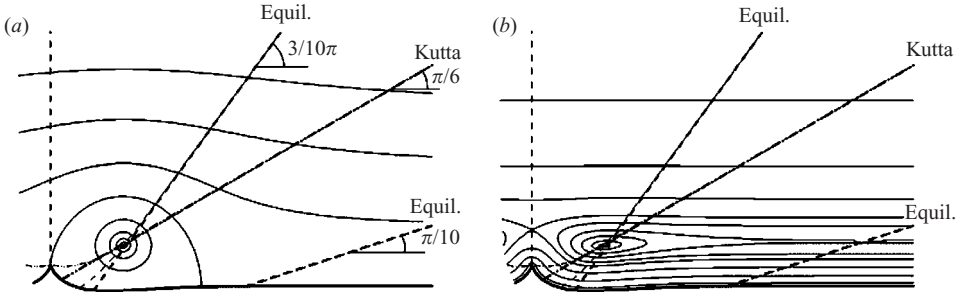

FIGURE 12. Kutta and equilibrium manifolds and asymptotes for the $N = 3$ cornice. (a) streamlines, (b) Hamiltonian contour lines for $\kappa/q = -8.788$.

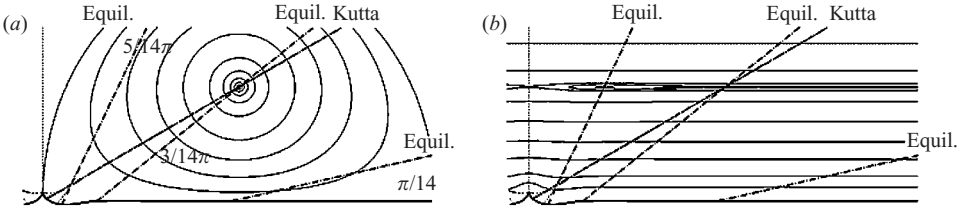

FIGURE 13. Kutta and equilibrium manifolds and asymptotes for the $N = 5$ cornice. (a) streamlines, (b) Hamiltonian contour lines for $\kappa_2/q = -32.964$.

the Kutta manifold ($z_0 = 2.184 + 1.259\,\mathrm{i}$). The relevant vortex circulation is $\kappa/q = -16.411$. The streamline pattern is shown on figure 11(a), while the Hamiltonian contour lines are drawn on figure 11(b).

For $N = 3$, the equilibrium manifold has two branches in the first quadrant with asymptotes defined by $\varphi_{eq_1} = \pi/10$ (unstable equilibrium branch) and $\varphi_{eq_2} = 3/10\pi$ (stable equilibrium branch). As shown in figure 12, there is a single intersection of the second branch with the Kutta manifold at $z_0 = 1.142 + 0.637\,\mathrm{i}$ with vortex circulation $\kappa/q = -8.788$.

The Kutta manifold asymptote, for the considered mapping (5.11), is the $y = \tan(\pi/6)x$ line, while the equilibrium manifold branch asymptotes are the $y = \tan(\varphi_{eq})\,x - 1$ lines. The first quadrant equilibrium asymptotes intersect the Kutta asymptote if $\varphi_{eq} > \pi/6$.

The manifold intersections are always close to the asymptote intersections, becoming closer and closer as N increases. Therefore, it is to be expected that the equilibrium manifold branches pertinent to $\varphi_{eq} > \pi/6$ undergo intersections with the Kutta manifold, while those pertinent to $\varphi_{eq} \leqslant \pi/6$ do not. The $N = 3$ case (figure 12) is an example of this behaviour. As a further example, let us consider the $N = 5$ case. This has three equilibrium manifold branches in the first quadrant whose asymptotic slopes are $\varphi_{eq_1} = \pi/14$ (stable), $\varphi_{eq_2} = 3/14\pi$ (unstable), $\varphi_{eq_3} = 5/14\pi$ (stable), respectively. The first branch does not intersect the Kutta manifold, while the other two branches intersect it at $z_{0_2} = 4.544 + 2.623\,\mathrm{i}$, with $\kappa_2/q = -32.964$ and $z_{0_3} = 0.612 + 0.320\,\mathrm{i}$, with $\kappa_3/q = -4.810$, respectively. Figure 13 shows the intersection of the unstable branch, and figure 14 the intersection of the stable branch of the equilibrium manifold with the Kutta manifold. The streamline patterns show that the Kutta condition is satisfied while the vortex Hamiltonian contour lines show the nature of the equilibrium.

The number of equilibrium branches asymptoting to $\varphi_{eq} > \pi/6$ increases with N and, as a consequence, the number of standing vortices that satisfy the Kutta condition

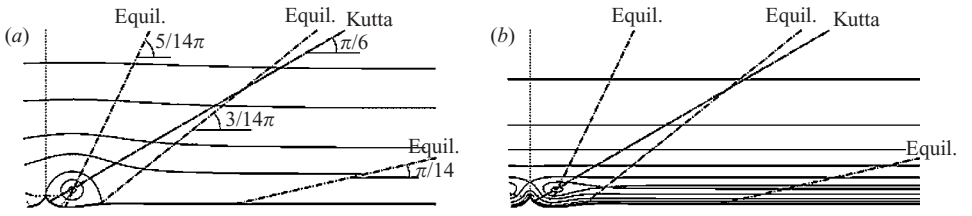

FIGURE 14. Kutta and equilibrium manifolds and asymptotes for the $N = 5$ cornice. (a) streamlines, (b) Hamiltonian contour lines for $\kappa_3/q = -4.818$.

also increases. For $N \to \infty$, the boundary becomes the real axis of the z-plane, and the Kutta manifold coincides with the $y = \tan(\pi/6)\,x$ line and it is the locus of standing vortices for a flow separation at $z_T = 0$.

The Kutta condition is a way of modelling the separation that occurs at a sharp edge. Since separation takes place at sharp edges in the real world, the existence of very similar geometries that allow, or do not allow, standing point vortices to satisfy the Kutta condition may seem odd. It is known that, depending on the geometry, not all obstacles admit a finite-area wake. Since the point vortex is a model for a region with closed streamlines, the above analysis suggests the geometrical property of a class of obstacles that admit, or do not admit, a finite-area wake.

Moreover, during the review process, one referee remarked on the difference between 'wall' and 'body', observing that all the described $N = 1$ walls can be seen as the upper half of bodies which are symmetric with respect to the real axis. On the other hand, the $N > 1$ walls have sections below their $y = 0$ asymptote and cannot be considered as the upper halves of non self-intersecting bodies. The referee suggested that the conjecture about the non-existence of standing vortices that satisfy the Kutta condition may still be valid for bodies which are symmetric with respect to the x- and y-axes.

6. Conclusions

The analysis has been carried out in the highly idealized framework of two-dimensional potential flow and point vortices.

The equilibrium conditions of a point vortex in a flow past a locally deformed wall have been studied. Equilibrium locations have been represented as fixed points of the vortex Hamiltonian contour line map. By analogy with the equilibrium condition of a point vortex in swirling flow past cylinders, it has been shown that such locations on the Hamiltonian map correspond to conditions of stable and unstable equilibrium, in a pattern that can be related to the Poincaré–Birkhoff fixed-point theorem. Once the physical z-plane is mapped onto a transformed ζ-plane, the Routh (1881) rule provides the main tool to study the vortex equilibrium condition. The two equations that define vortex equilibrium have been put in a form such that the first one (3.4) only depends on the body geometry and defines the manifold which is the locus of the vortex equilibrium, equivalent to the Föpple curve for semicircular bumps, while the second equation (3.5) is written in a form that defines the vortex circulations.

By considering the complex potential $\tilde{w}(z)$ of the pure potential flow, an equivalent result for the vortex equilibrium locus (3.9) and vortex circulations (3.12) can be obtained together with a kinematical property (3.10) of the equilibrium manifold.

The requirement that the flow separates at a given point, that is, the enforcement of the Kutta condition, defines a Kutta manifold, whose first quadrant branch has the asymptotic direction $\varphi_{Kutta} = \pi/6$. The intersections of the Kutta manifold with

the equilibrium manifold are the locations of standing vortices that satisfy the Kutta condition.

The existence of standing vortices that satisfy the Kutta condition for symmetric bodies has been related to the value N of the index of the first non-null term in the mapping expansion (5.8). It has been argued that for $N=1$ there are no such vortices, while they exist for $N>1$ and their number increases with N. For $N\to\infty$ the body reduces to a flat plate, the Kutta manifold reduces to its general asymptote $y=x/\sqrt{(3)}$ and it is the locus of standing vortices for flows separating at $z=0$.

REFERENCES

Batchelor, G. K. 1956 On steady laminar flows with closed streamlines at large Reynolds number. *J. Fluid Mech.* **1**, 177–190.

Cai, J., Liu, F. & Luo, S. 2003 Stability of symmetric vortices in two dimensions and over three-dimensional slender conical bodies. *J. Fluid Mech.* **480**, 65–94.

Chernyshenko, S. I. 1991 Separated flow over a backward-facing step whose height is much greater than the thickness of the lower sublayer of the interaction zone. *Fluid Dyn. Res.* **26**(4), 496–501.

Chernyshenko, S. I., Galletti, B., Iollo, A. & Zannetti, L. 2003 Trapped vortices and a favorable pressure gradient. *J. Fluid Mech.* **482**, 235–255.

Childress, S. 1966 Solutions of Euler equations containing finite eddies. *Phys. Fluids* **9**, 860–872.

Clements, R. R. 1973 An inviscid model of two-dimensional vortex shedding. *J. Fluid Mech.* **57**, 321–336.

Cortelezzi, L., Chen, Y. C. & Chang, H. L. 1997 Nonlinear feedback control of the wake past a plate: from a low-order model to a higher-order model. *Phys. Fluids* **9**, 2009.

Crowdy, D. & Marshall, J. 2004 Growing vortex patches. *Phys. Fluids* **16**, 3122–3129.

Deem, G. S. & Zabusky, N. J. 1978 Vortex waves: Stationary V states, interactions, recurrence, and breaking. *Phys. Rev. Lett.* **40**, 859–862.

Elcrat, A., Forneberg, B., Horn, M. & Miller, K. 2000 Some steady vortex flows past a circular cylinder. *J. Fluid Mech.* **409**, 13–27.

Elcrat, A. R., Hu, C. & Miller, K. G. 1997 Equilibrium configurations of point vortices for channel flows past interior obstacles. *Eur. J. Mech.* B/*Fluids* **16**, 277–292.

Föppl, L. 1913 Wirbebewegung hinter einem kreiszylinder. *Sitzb. d. k. Bayer, Akad. d. Wiss., Math-Physi. Klasse, München* **1**, 1–17.

Gallizio, F. 2004 Modello di Prandtl-Batchelor per il flusso normale ad una placca piana posta all'interno di un canale: studio numerico dell'esistenza e unicità della soluzione. Dissert. Tesi Laurea Ing. Aerosp. aa 2003/2004, Politecnico di Torino, Turin, Italy.

Ives, D. C. 1976 A modern look at conformal mapping, including multiply connected regions. *AIAA J.* **14**, 1006–1011.

Meleshko, V. V. & van Heijst, G. J. F. 1994 Interacting two-dimensional vortex structures: point vortices, contour kinematics and stirring properties. *Chaos, Solitons & Fractals* **4**, 977–1010.

Pierrehumbert, R. T. 1980 A family of steady, translating vortex pairs with distributed vorticity. *J. Fluid Mech.* **99**, 129–144.

Protas, B. 2004 Linear feedback stabilization of laminar vortex shedding based on a point vortex model. *Phys. Fluids* **16**, 4473–4488.

Ringleb, F. O. 1961 Separation control by trapped vortices. *Boundary Layer and Flow Control* (ed. G. V. Lachman), pp. 265–294, Pergamon.

Routh, E. J. 1881 Some application of conjugate functions. *Proc. Lond. Math. Soc.* **12**, 73–89.

Sadovskii, V. S. 1971 Vortex regions in a potential stream with a jump of Bernoulli's constant at the boundary. *Appl. Math. Mech* **35**, 729–735.

Saffman, P. G. 1992 *Vortex Dynamics*. Cambridge University Press.

Saffman, P. G. & Tanveer, S. 1982 The touching pair of equal and opposite uniform vortices. *Phys. Fluids* **25**, 1929–1930.

Smith, J. H. B. 1986 Vortex flows in aerodynamics. *Annu. Rev. Fluid Mech.* **18**, 221–242.

Smith, J. H. B. & Clark, R. W. 1986 Nonexistence of stationary vortices behind a two-dimensional normal plate. *AIAA J.* **13**, 1114–1115.

Tabor, M. 1989 *Chaos and Integrability in Non Linear Dynamics*. Wiley.

Theodorsen, T. & Garrick, I. E. 1934 General potential theory of wing sections. *NACA Tech. Rep.* 452.

Turfus, C. 1993 Prandtl-Batchelor flow past a flat plate at normal incidence in a channel – inviscid analysis. *J. Fluid Mech.* **249**, 59–72.

Zannetti, L. & Chernyshenko, S. 2005 Vortex pair and Chaplygin cusps. *Eur. J. Mech.* B/*Fluids* **24**, 328–337.

Zannetti, L. & Franzese, P. 1994 The non-integrability of the restricted problem of two vortices in closed domains. *Physica* D **76**, 99–109.

Zannetti, L. & Iollo, A. 2003 Passive controlof the vortex wake past a flat plate at incidence. *Theor. Comput. Fluid Dyn.* **16**, 211–230.